View metadata, citation and similar papers at core.ac.uk

brought to you by CORE

provided by Caltech Authors

ACS APPLIED ENERGY MATERIALS

Caltech Library

Subscriber access provided by Caltech Library

Article

Autonomous Light Management in Flexible Photoelectrochromic Films Integrating High Performance Silicon Solar Microcells

Maggie Michelle Potter, Mikayla A. Yoder, Aaron Petronico, Sean E. Lehman, Bruno Giuliano Nicolau, Michael J. Enright, Megan Phelan, Junwen He, Harry A Atwater, and Ralph G Nuzzo

ACS Appl. Energy Mater., **Just Accepted Manuscript** • DOI: 10.1021/acsaem.9b01987 • Publication Date (Web): 31 Jan 2020

Downloaded from pubs.acs.org on January 31, 2020

Just Accepted

"Just Accepted" manuscripts have been peer-reviewed and accepted for publication. They are posted online prior to technical editing, formatting for publication and author proofing. The American Chemical Society provides "Just Accepted" as a service to the research community to expedite the dissemination of scientific material as soon as possible after acceptance. "Just Accepted" manuscripts appear in full in PDF format accompanied by an HTML abstract. "Just Accepted" manuscripts have been fully peer reviewed, but should not be considered the official version of record. They are citable by the Digital Object Identifier (DOI®). "Just Accepted" is an optional service offered to authors. Therefore, the "Just Accepted" Web site may not include all articles that will be published in the journal. After a manuscript is technically edited and formatted, it will be removed from the "Just Accepted" Web site and published as an ASAP article. Note that technical editing may introduce minor changes to the manuscript text and/or graphics which could affect content, and all legal disclaimers and ethical guidelines that apply to the journal pertain. ACS cannot be held responsible for errors or consequences arising from the use of information contained in these "Just Accepted" manuscripts.

is published by the American Chemical Society. 1155 Sixteenth Street N.W., Washington, DC 20036

Published by American Chemical Society. Copyright © American Chemical Society. However, no copyright claim is made to original U.S. Government works, or works produced by employees of any Commonwealth realm Crown government in the course of their duties.

Autonomous Light Management in Flexible Photoelectrochromic Films Integrating High Performance Silicon Solar Microcells

*Maggie M. Potter,[1†] Mikayla A. Yoder, [2†] Aaron Petronico, [2] Sean E. Lehman, [2] Bruno G. Nicolau, [2] Michael J. Enright,[2] Megan Phelan,[3] Junwen He, [2] Harry A. Atwater,[3] Ralph G. Nuzzo[2,4]**

Ms. M. M. Potter
Department of Chemical and Biomolecular Engineering, University of Illinois at Urbana-Champaign, Urbana, Illinois 61801, USA.

Dr. M. A. Yoder, Dr. A. Petronico, Dr. S. E. Lehman, Dr. B. G. Nicolau, Dr. M. J. Enright, Dr. J. He, Prof. R. G. Nuzzo
School of Chemical Sciences, University of Illinois at Urbana-Champaign, Urbana, Illinois 61801 USA

Ms. M. Phelan, Prof. H. A. Atwater
Thomas J. Watson Laboratories of Applied Physics, California Institute of Technology, Pasadena, CA 91125, USA

Prof. R. G. Nuzzo
Surface and Corrosion Science, School of Engineering Sciences in Chemistry, Biotechnology and Health, KTH Royal Institute of Technology, Drottning Kristinasväg 51, 100 44 Stockholm, Sweden

E-mail: r-nuzzo@illinois.edu

[†]Authors contributed equally to the work.

Keywords: *photoelectrochromic windows, smart windows, photovoltaics, electrochromic devices, micro-cells*

Abstract: Commercial smart window technologies for dynamic light and heat management in building and automotive environments traditionally rely on electrochromic (EC) materials powered by an external source. This design complicates building-scale installation requirements and substantially increases costs for applications in retrofit construction. Self-powered photoelectrochromic (PEC) windows are an intuitive alternative wherein a photovoltaic (PV) material is used to power the electrochromic device, which modulates the transmission of the incident solar flux. The PV component in this application must be sufficiently transparent and

produce enough power to efficiently modulate the EC device transmission. Here, we propose Si solar microcells (μ-cells) that are i) small enough to be visually transparent to the eye, and ii) thin enough to enable flexible PEC devices. Visual transparency is achieved when Si μ-cells are arranged in high pitch (i.e. low-integration density) form factors while maintaining the advantages of a single-crystalline PV material (i.e., long lifetime and high performance). Additionally, the thin dimensions of these Si μ-cells enable fabrication on flexible substrates to realize these flexible PEC devices. The current work demonstrates this concept using WO_3 as the EC material and V_2O_5 as the ion storage layer, where each component is fabricated via sol-gel methods that afford improved prospects for scalability and tunability in comparison to thermal evaporation methods. The EC devices display fast switching times, as low as 8 seconds, with a modulation in transmission as high as 33%. Integration with two Si μ-cells in series (affording a 1.12 V output) demonstrates an integrated PEC module design with switching times of less than 3 minutes, and a modulation in transmission of 32% with an unprecedented EC:PV areal ratio.

1. Introduction

In the United States, internal lighting, heating, ventilation, and air conditioning (HVAC) systems account for ca. 30% of total energy demand, and the development of building-integrable technologies to aid in mitigation of energy consumption presents a holistic design challenge.[1-4] One approach that allows for specific control over internal lighting and heating/cooling needs are smart windows, which offer tunable and dynamic alternatives to traditional paned windows. Electrochromic (EC) windows, a subset of smart window technologies, dynamically control the transmitted solar flux by either absorbing or reflecting a portion of the incident solar spectrum via manipulation of an externally applied bias. Selective transmission of visible and infrared (IR)

wavelengths facilitates control over lighting and heating/cooling needs, thereby reducing energy consumption.[1, 5-7]

EC materials have been explored in research since the early 1960s[8-10] and their integration into windows intensively examined in the 1980s – early 2000s,[11-16] however, widespread commercialization has been frustrated by the need for complicated internal wiring and complete reinstallation of existing windows.[14] PV-powered EC windows are an intuitive solution that utilize incident solar irradiation to power the EC window and circumvent some of the complexity associated with internal wiring. Typical power requirements for EC films are quite low, with switching voltages on the order of 1.0 V,[16-17] facilitating integration with transparent and/or low-cost PV materials. Here, we use Si solar μ-cells that offer high power density and a level of

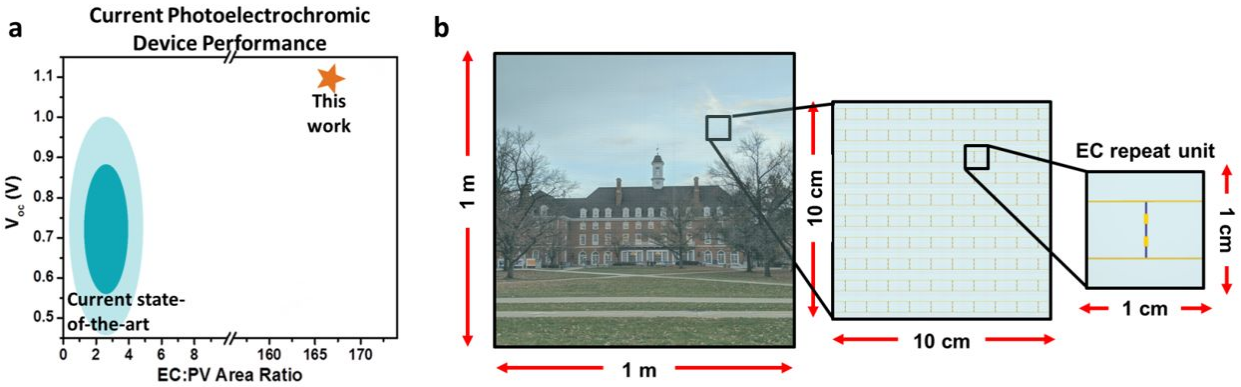

Figure 1. (a) Current PEC devices (blue) with dark blue corresponding to where most PEC devices lie. Our work is shown for comparison (orange star). (b) Schematic of interconnected Si solar μ-cells in comparison to a 1 m^2 window demonstrating their high transparency.

transparency based on the density of μ-cells needed for fast switching times and high modulation of transmission.[18] These μ-cells have an area of only 0.003 cm^2 (1.5 mm x 200 μm), yet produce a V_{OC} of 0.55 V with power conversion efficiencies of 13.7%.[18] To power a typical 1 cm^2 EC device at 1.0 V, two μ-cells in series (V_{OC} ca. 1.1 V) amount to an area of 0.006 cm^2 and an EC:PV areal ratio (ratio of EC device area to PV device area) of 166. **Figure 1a** illustrates this work in comparison to the literature; typical power requirements necessitate larger area PV, and

significant efforts have been made to produce impressive results with either integrated or side-by-side PV materials. Namely, Si-based semitransparent thin films,[13, 16, 19-21] transparent or UV/NIR selective polymers,[1, 22-23] dye sensitized solar cells (DSSCs),[24-25] InGaN-based materials,[26] and thin film perovskites[27] have been applied to provide self-powering for EC devices. Here, we look instead to microscale, high performance, single-crystalline Si and optimize optical absorption and electrical performance to effect transparency. This concept is illustrated in **Figure 1b**, where the form factor of a 1 cm^2 device is shown schematically on the right. Expanding the device area and replicating 1 cm^2 devices to power a larger area results in a pattern much like a window screen with minimal visual obscurity.

In addition to the PV component, the EC materials are chosen specifically for ease of processing and scalability. In this demonstration we apply tungsten (VI) oxide (WO_3) and vanadium (V) oxide (V_2O_5) as the electrochromic and ion storage layers, respectively. Both materials are prepared via sol-gel chemistry and thin-film coatings are optimized purposefully for use in a flexible device format. The form factor of the active layers permits facile integration on a flexible polymeric substrate—demonstrated here using a material suitable for use as a laminate against glass. This method of preparation enables fabrication within ambient (i.e. non-vacuum) environments and can be easily adapted to scalable, roll-to-roll processing. In combination with capabilities for deterministic assembly of the Si μ-cell components onto polymeric and/or thin-glass substrates,[28-35] we demonstrate a prototype for a self-powered, flexible device that can be retrofitted to existing windows via an adhesive layer applied on one side of the device.

2. Results and Discussion

2.1. Electrochromic Layer Fabrication and Gel Electrolyte Characterization

The structure of the EC device comprises an electrochromic layer, an ion storage layer, and a gel electrolyte between the two. This composition can be seen in **Figure 2a**, where WO_3 is the electrochromic material and V_2O_5 is the complementary material, or ion storage layer. An external bias causes lithiation of the electrochromic or ion storage layer, resulting in either coloration or bleaching (**Figure 2b**), respectively. The redox reactions of both layers are as follows:

$$WO_3 + x(Li^+ + e^-) \rightleftarrows Li_xW^{VI}_{(1-x)}W_x^{V}O_3$$

$$Li_xV^{IV}_{(1-x)}V_x^{V}O_5 \rightleftarrows V_2O_5 + x(Li^+ + e^-)$$

where the left side of the reaction corresponds to the bleached state and the right side to the absorptive state.

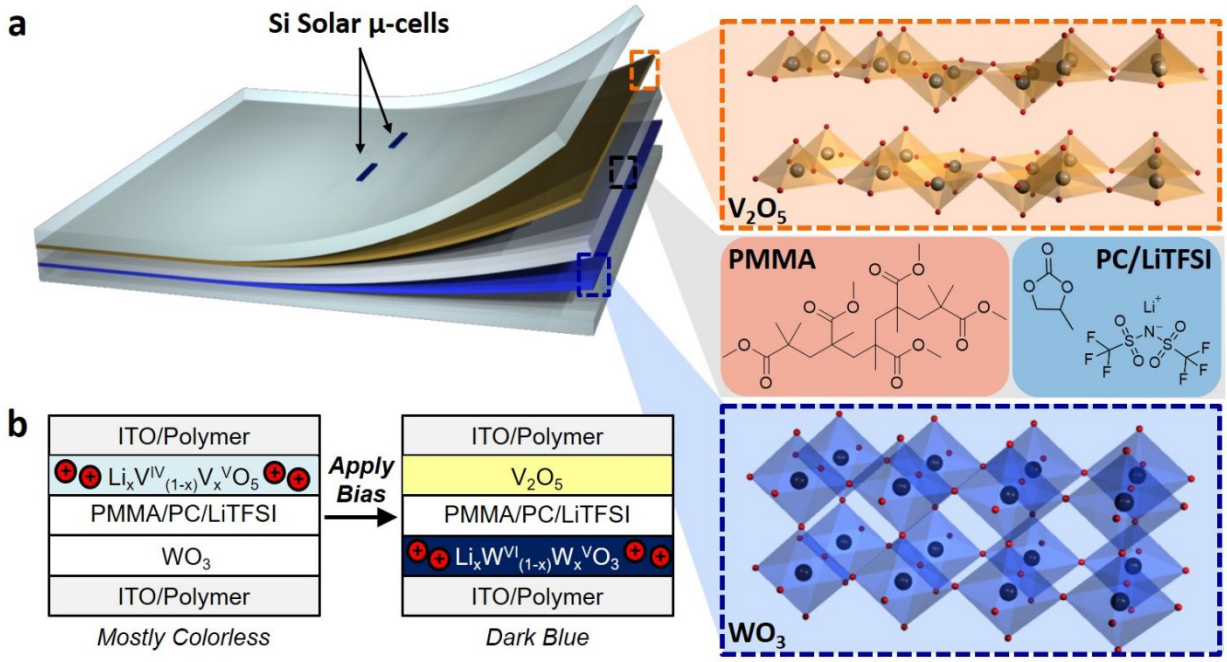

Figure 2. (a) Flexible PEC device schematic. (b) EC device operation highlighting the bleached (left) and absorptive (right) states.

Movement of lithium ions is facilitated through a gel electrolyte. Specifically, we use a 1 M solution of LiTFSI in propylene carbonate (PC) and mix the solution with a high molecular

weight poly(methyl methacrylate) (PMMA) network, as described in detail in the Supplementary Information.[36] Gel electrolytes combine advantages of liquid and solid electrolytes by providing higher conductivities while remaining mechanically robust. We found that solid electrolytes demonstrated ionic conductivities too low to allow facile lithiation and delithiation of the metal oxide films.

Each metal oxide film was prepared via sol-gel methods on ITO-coated (glass or polymer) substrates, ultimately forming the oxide network via hydrolysis/condensation of the respective metal alkoxide. This type of preparation allows for ease of processing and scalability as compared to typical thermal evaporation of the respective powders.[37] Here, WO_3 was prepared from $WOCl_4$ powder, which was reacted with isopropyl alcohol (IPA) to form the alkoxide. The alkoxide was then spin-coated and hydrolyzed under ambient conditions; thermal annealing at 150°C drove off residual solvent. The nature of these thin film materials is established by the data presented in **Figure 3(a-i)**. An example of a spin-coated WO_3 film on ITO/glass is shown in **Figure 3a**. Similarly, V_2O_5 was prepared from $VO(OC_3H_7)_3$, which also hydrolyzed in ambient with the addition of acetic acid as a catalyst. The film was then spin-coated and annealed at 300 °C under O_2 flow; an as prepared V_2O_5 thin film is shown in **Figure 3b**. Additional layers built up thicknesses of each film to the final thicknesses of ca. 160 – 270 nm. The XRD patterns in **Figure 3c** suggest that the WO_3 film is amorphous, with observed peaks attributed to the underlying indium tin oxide (ITO, shown in black), while the V_2O_5 is semi-crystalline. The pattern for V_2O_5 shows several peaks for crystalline V_2O_5, specifically peaks that can be indexed to the (200), (001), and (002) crystal planes (**Figure 3c**, shown in blue). This difference in crystallinity between the two oxide films could influence lithium ionic conductivity and the ability to balance charge during device operation, however, we do not observe much of a

perturbation in our device, as described below. Representative SEM images in **Figure 3e** and **Figure 3h** of the WO_3 and V_2O_5 films, respectively, confirm that each oxide film is continuous

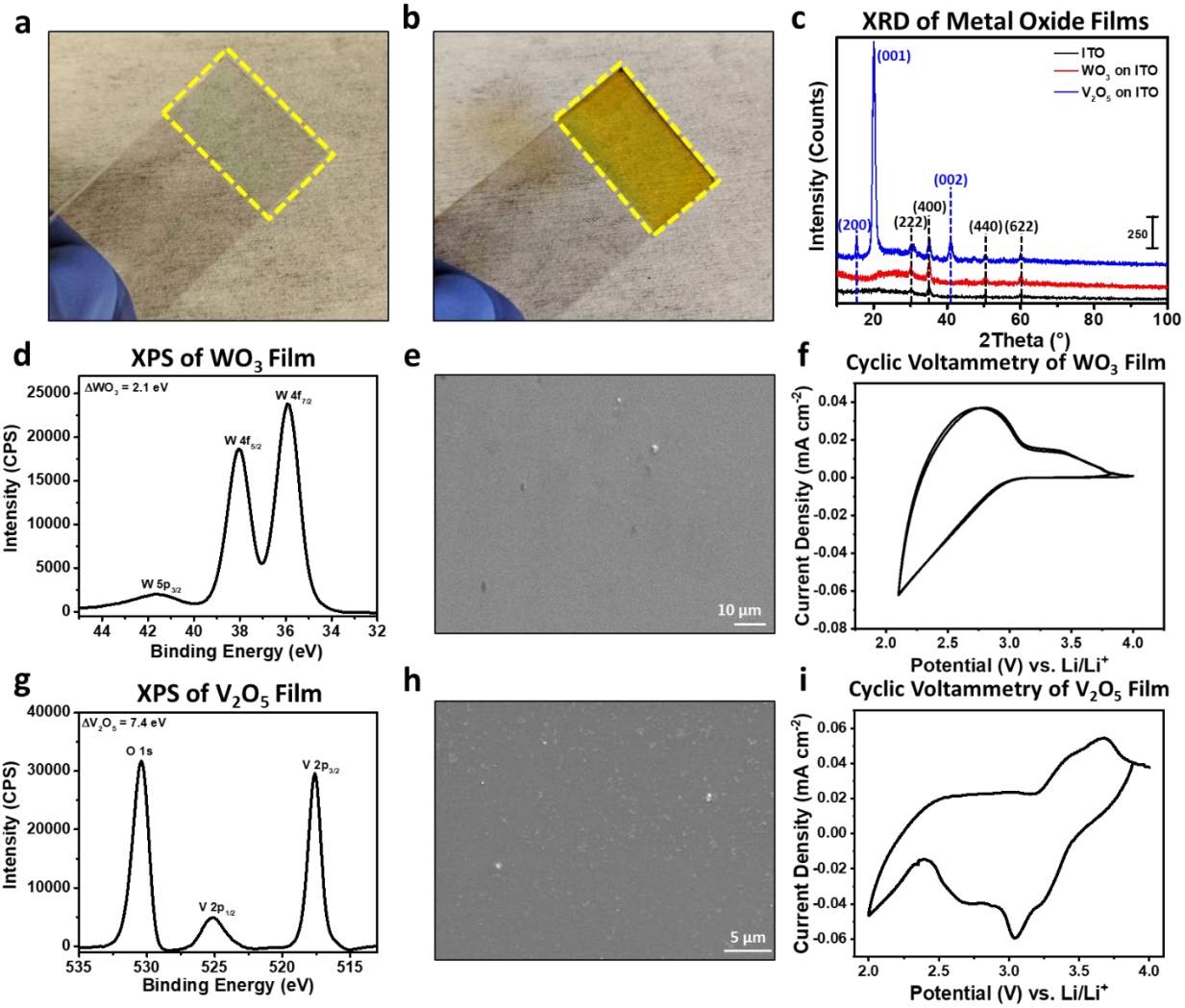

Figure 3. EC materials characterization. Images of the as-deposited (a) WO_3 and (b) V_2O_5 films. (c) XRD of WO_3 on ITO (red), V_2O_5 on ITO (blue), and ITO (black). (d-i) Characterization of WO_3 (d-f) and V_2O_5 (g-i) films including (d, g) XPS, (e, h) SEM, and (f, i) cyclic voltammetry with gel electrolyte vs. lithium metal (1 mV/s scan rate).

and homogeneous through the extent of the coated surfaces.

Characterization of the metal oxide films with XPS provides a speciation of the oxidation states of each metal. As seen in **Figure 3d**, the WO_3 film displays the doublet for the W4f core levels at binding energies of 38.0 and 35.9 eV for the W $4f_{5/2}$ and W $4f_{7/2}$ peaks, respectively. The

W $5p_{3/2}$ peak is also observed at 41.6 eV. These values agree well with reported values for tungsten(VI).[38] The spectrum for the V_2O_5 sample, **Figure 3g**, also matched well with literature data for single phase compositions of this material,[39] with characteristic peaks for O 1s at 530.5 eV, V $2p_{1/2}$ at 525.0 eV, and V $2p_{3/2}$ at 517.6 eV.[40] The fits of both spectra are presented in **Figure S1(a-b)** of the Supplementary Information.

Cyclic voltammetry was performed for each oxide film using both liquid and gel electrolytes. All half-cell voltammograms were measured using Li metal as a reference and counter electrode. **Figure 3f** shows the voltammogram for a 230-nm thick WO_3 film cycled with a 35 wt.% PMMA gel electrolyte (described below) at 1 mV s^{-1}. Observed peaks for oxidation and reduction correspond well with observed color changes from transparent to deep blue, behaviors also seen in the voltammogram cycled in liquid electrolyte (0.1 M $LiClO_4$ in PC, 50 mV s^{-1}) as shown in the data presented in **Figure S2a** of the Supplementary Information. The voltammogram in **Figure 3i** displays a 268 nm-thick V_2O_5 film cycled with the 35 wt.% PMMA gel electrolyte at 1 mV s^{-1} and shows multiple peaks during lithiation and delithiation, corresponding to structural phase changes within the film.[41] When cycled in liquid electrolyte (1.0 M $LiClO_4$ in PC, 1 mV s^{-1}, **Figure S2b**), these peaks are sharper and are shifted slightly due to faster mass transport in liquid electrolyte. Charge injected based on the cyclic voltammograms in **Figure 3** is shown in **Table S1**. To balance the WO_3 and V_2O_5 films for performance in the EC device,[42] the V_2O_5 layer thickness was reduced to 166 nm and the resulting inserted charge was assessed during reduction of each film at a slower scan rate of 0.1 mV/s (**Table S1** and **Figure S3**).

To optimize a balance between ionic conductivity and mechanical robustness of the gel electrolyte material, two different weight percent solutions of the gel electrolyte were prepared:

30 wt.% and 35 wt.% PMMA (M_W = 120,000 Da) mixed with 1 M LiTFSI in PC. Electrical impedance was measured for each mixture [Figure S4(a-b), Supplementary Information] in a symmetric cell with two steel electrodes. The 30 wt.% PMMA mixture had a measured conductivity two times higher than that of the 35 wt.% PMMA mixture, but both resided close to 10^{-4} S cm^{-1}. Additionally, rheology measurements revealed that the 35 wt.% mixture had a modulus five times that of the lower weight percentage mixture (3177 Pa·s and 616 Pa·s for 35 wt.% and 30 wt.%, respectively). Considering the ionic conductivity of the 35 wt.% PMMA gel electrolyte is high enough for our application and the modulus is significantly higher, we continued the work using the 35 wt.% PMMA gel electrolyte exclusively. The data in Figure S4c show the high transmission of the gel electrolyte throughout the working wavelength regime (300-2000 nm) of our device apart from a few small peaks due to absorbance from functional groups (e.g., carbonyl) in the PMMA and LiTFSI. The stability window of the gel electrolyte (Figure S4d) shows that the electrolyte is suitable for use within the operating voltage range of the EC device, and produces currents on the order of uA cm^{-2} between 2 – 4.5 V vs. Li/Li^+ (vide supra).

2.2. Electrochromic Device Fabrication and Characterization

Assembly of the EC device is explained in detail in the Supplementary Information. Briefly, a substrate-supported WO_3 film is first reduced and sandwiched with a similarly deposited V_2O_5 film that has the 35 wt.% PMMA gel electrolyte cast atop it and molded to a limiting thickness established by 100 μm glass bead spacers. The entire device is encapsulated with NOA61 in an inert environment to prevent oxygen permeating into the device and oxidizing of the pre-reduced WO_3 film. **Figure 4a** and **Figure 4b** show images of an assembled device on ITO/glass in the bleached (**Figure 4a**) and absorptive (**Figure 4b**) states. The transmission modulation is apparent

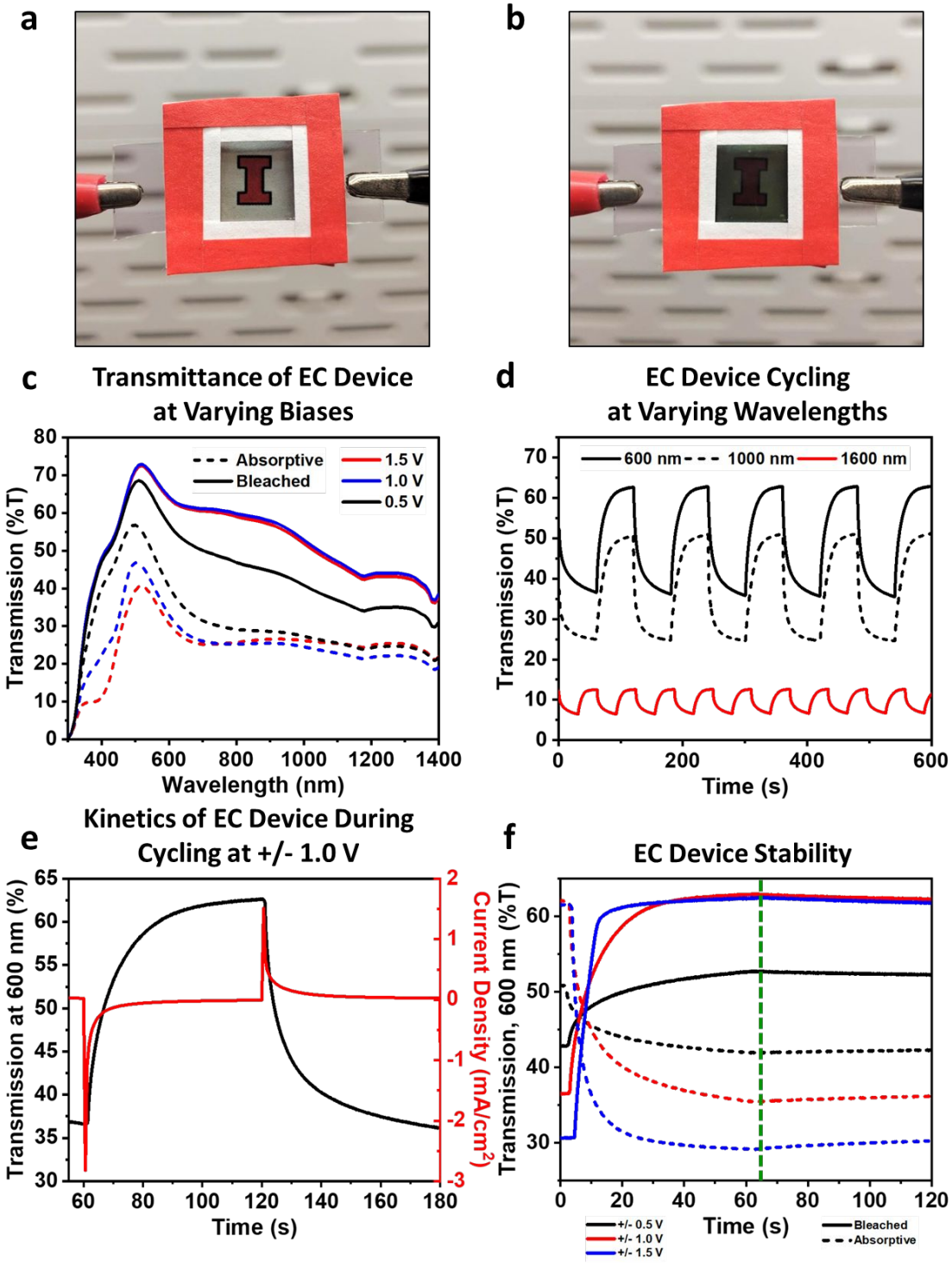

Figure 4. EC performance. Images of the bleached (a) and absorptive (b) EC device; university logo used with permission from the University of Illinois. (c) Transmission of the EC device with varying bias. (d) EC device cycling between +/- 1.0 V monitored at 600 nm (black, solid), 1000 nm (black, dashed), and 1600 nm (red, solid). (e) One cycle of the EC device showing transmission at 600 nm (black) and corresponding current (red). (f) Bias holds of the EC device monitored at 600 nm for bleached (solid) and absorptive (dashed) states. The green dashed line indicates when the bias was removed.

in these images and is quantified in the spectra shown in **Figure 4c**, using an ITO-based 100% T reference spectrum as described in detail in the supporting information (**Figure S5** and **Figure S6)**. Here, the device is biased at voltages corresponding approximately to the V_{OC} of one, two, and three Si μ-cells interconnected in series, or 0.5 V, 1.0 V, and 1.5 V, respectively. As shown in the spectra, a bias of 0.5 V does not produce a large change in transmittance, with a ΔT_{max} of only 10 – 20% due to incomplete coloration/decoloration of the EC device. The modulation is significantly increased when using either a 1.0 V or 1.5 V bias. Due to the rather small enhancement of ΔT_{max} when comparing the 1.0 V and 1.5 V bias and the additional complexity of connecting three instead of two Si μ-cells in series, we pursued the testing of an EC pixel module (e.g., **Figure 2a**) that was powered by two Si μ-cells in series. The kinetics of the device can be analyzed by monitoring transmittance at specific wavelengths while cycling between a positive and negative bias. The results for a bias of 1.0 V are shown in **Figure 4d**, and **Table 1** summarizes performance characteristics at each bias (i.e., 0.5 V, 1.0 V, and 1.5 V), where transmission is monitored at three wavelengths across the spectrum relevant to either visible light or heat management: 600 nm, 1000 nm, and 1600 nm. A video demonstrating the switching times for coloration and bleaching upon application of an external bias (1.5 V) is provided in the supporting information. The ITO transmission spectrum on glass and full cycles for each bias and wavelength can be seen in **Figure S7(a-d)** in the Supplementary Information. It is evident in **Figure 4d** that performance at infrared wavelengths (i.e., 1600 nm) is adversely impacted by the relatively low transmission of the conductive ITO coating. EC devices are commonly prepared with ITO as a transparent electrode,[1, 13, 15, 22, 43-46] however, it is clearly not an ideal choice when attempting to modulate heat and infrared influx in the built environment. Potential alternatives to ITO include conductive polymers,[47-49] carbon-based electrodes,[50-51] and thin metal films or

nanostructures,[52] but these tend to lack in conductivity and/or transparency. To holistically optimize the design of EC device architecture, an IR-transmissive conductor is preferable for high modulation capacities at longer wavelengths and should be a subject of future research efforts to improve capability for dynamically effective heat management.

As seen in **Table 1**, ΔT_{max} is correlated with the applied voltage. At 600 nm, ΔT_{max} increases from 16.5% to 33.2% with a 0.5 V and 1.5 V bias, respectively. The change in optical

Table 1. Performance parameters of EC device at varying wavelength and bias.

Bias (V)	Coloration Time (sec)	Bleaching Time (sec)	ΔT_{max}(%)	ΔOD	Coloration Efficiency (cm^2/C)
λ = 600 nm					
0.5 V	34.0	36.9	16.5	0.096	43.2
1.0 V	26.8	23.7	31.3	0.248	41.7
1.5 V	13.3	8.1	33.2	0.330	29.0
λ = 1000 nm					
0.5 V	25.3	38.4	13.5	0.134	49.4
1.0 V	16.2	25.4	28.3	0.317	50.6
1.5 V	5.8	15.3	25.7	0.343	30.6
λ = 1600 nm					
0.5 V	20.8	21.8	3.35	0.085	41.9
1.0 V	18.5	14.5	6.96	0.281	46.0
1.5 V	7.2	9.3	6.59	0.333	29.3

density, ΔOD, follows with ΔT_{max} and is used to calculate the coloration efficiency, η:

$$\Delta OD = \log \frac{T_{bleached}}{T_{colored}}$$

$$\eta = \frac{\Delta OD}{Q}$$

where Q is the charge injected in C cm^{-2}. Of note is that η does not follow the same trend as that of ΔT_{max} and ΔOD; with an applied bias of 1.5 V, η decreases significantly. This is likely because the ΔT_{max} of the WO_3 electrochromic layer is reached before 1.5 V and the excess charge that is injected is essentially wasted; the ΔT_{max} of the WO_3 film could be increased with a thicker film to mitigate this.

Figure 4e shows one cycle of the EC device between +1.0 V and -1.0 V plotted with the current density for a 60 second bias hold. The current density follows a capacitor-like behavior in which the device initially charges, corresponding to the large increase in the magnitude of the current density. This is related to the switching time of the device, whereas the voltage is related to the attainable modulation in transmittance. The switching times, defined as $0.9*\Delta T_{max}$, can be found in **Table 1** for each bias. For 600 nm, the coloration time is as rapid as 13.3 seconds for a 1.5 V bias. The switching times increase as lower voltages are applied, increasing to 26.8 and 34.0 seconds for 1.0 V and 0.5 V biases, respectively. This agrees well with Ohm's law, $V = IR$, where a larger voltage corresponds to a larger current and therefore shorter switching times.

The difference between the bleaching and coloration times is negligible apart from the data taken at 1000 nm, where the bleaching time is longer. We explain this discrepancy by the difference in crystallinity between the two metal oxide films. It has been suggested that amorphous films can lead to faster switching times and facilitate charge injection/extraction.[11, 53] With this in mind, we hypothesize that the semi-crystalline V_2O_5 film kinetically limits the device to some degree, specifically at 1000 nm. While the diffusion coefficient of lithium ions is identical within the same film for processes observed at different wavelengths, the magnitude of transmission variation at each wavelength is different for the individual WO_3 and V_2O_5 films. **Figure S8(a-b)** in the Supplementary Information shows the transmission modulation of each

metal oxide film as measured by itself. The WO_3 layer demonstrates a large transmission modulation for each wavelength (600, 1000, 1600 nm) whereas the V_2O_5 layer only substantially modulates transmission at 1000 nm. Therefore, transmission modulation of the entire EC device is largely dependent on the WO_3 as the electrochromic material at 600 and 1600 nm, however, both layers have similar modulation at 1000 nm and the bleaching process here is limited by slow charge injection into V_2O_5.

Additionally, we observe asymmetric current density with time (**Figure 4e**) for each experiment; **Figure S9** in the Supplementary Information shows a detailed analysis of the integrated current and charge obtained over cycling. Here, coloration is observed to take longer than that for bleaching. This asymmetric current has previously been observed with WO_3, where the injection of lithium ions is simply suggested to take longer than extraction, but the magnitude of injected charge is symmetric.[11, 13] One potential explanation is that the coloration is limited by charge extraction from V_2O_5, resulting from changes in transport properties associated with the different crystalline phases induced by Li^+ injection/extraction.[41] Both bleached and absorptive states are sustained after the applied bias is removed, as seen in **Figure 4f**, where the bias is held for the first 60 seconds and then removed while the transmission is monitored continuously at 600 nm. Upon removal of the bias, a negligible change in transmission is observed, on the order of 1 – 2%, indicating the device displays optical memory. Notably, in this design continued illumination on the window corresponds to a continued applied bias by the integrated PV microcells, and therefore the transmission is expected to remain constant over long periods of time depending on the intensity of incident illumination. Illustrative plots of time dependent transmission monitored at 1000 nm and 1600 nm are given in **Figure S10(a-b)** in the Supplementary Information to further illustrate the limited rates of self-discharge seen in this

system.

2.3. Si Solar μ-cell Integration and Performance of the Photoelectrochromic Device

2.3.1. Si μ-cell Performance

Performance metrics of the Si μ-cells are discussed in detail in Ref. 18; here, we focus on the open circuit voltage and current density that drive EC device operation. The Si μ-cells are fabricated upside down to lithographically pattern the contacts; **Figure S11a** shows an image of a μ-cell array on the source wafer. After transfer printing, the μ-cell contacts are still facing upwards and JV curves are shown for this case as well as for fully interconnected and inverted μ-cells (i.e., contacts facing downwards). Noticeably, the J_{SC} and V_{OC} increase due to the reduced shading from the contacts when they are facing downward. Additionally, we show the JV curves of one and two Si μ-cells in series in **Figure S11b** and performance of two Si μ-cells in series under varying illumination conditions in **Figure S11c**. Connecting two Si μ-cells in series increases the V_{OC} from 0.566 to 1.12 V (**Figure S11b**). Decreased irradiation (e.g., less than 1 sun illumination) corresponds to non-ideal illumination conditions, and the Si μ-cells produce smaller currents shown in the curves (**Figure S11c**). **Figure S11d** shows modelling results of the anticipated EC device performance as a function of the number of Si μ-cells placed in series. The incident intensity on the external surface of the window, I_{ext}, is plotted versus the transmitted intensity through the EC window in the absorptive state, I_{int}. The internal intensity was calculated for an I_{ext} of 1000, 750, 500, and 250 W m^{-2} corresponding to 1, 0.75, 0.50, and 0.25 suns, respectively. Comparing one and three μ-cells in series, I_{int} decreases from 193 to 100 W m^{-2} with an I_{ext} of 1000 W m^{-2}. In general, the I_{int} decreases by an order of magnitude after passing through the window.

2.3.2. Integration of Si μ-cells with the Electrochromic Film

A schematic to illustrate the mechanism of transmission modulation of the EC component using the Si μ-cell array is shown **Figure 5(a-b)**. Here, we transfer print Si μ-cells in series on a

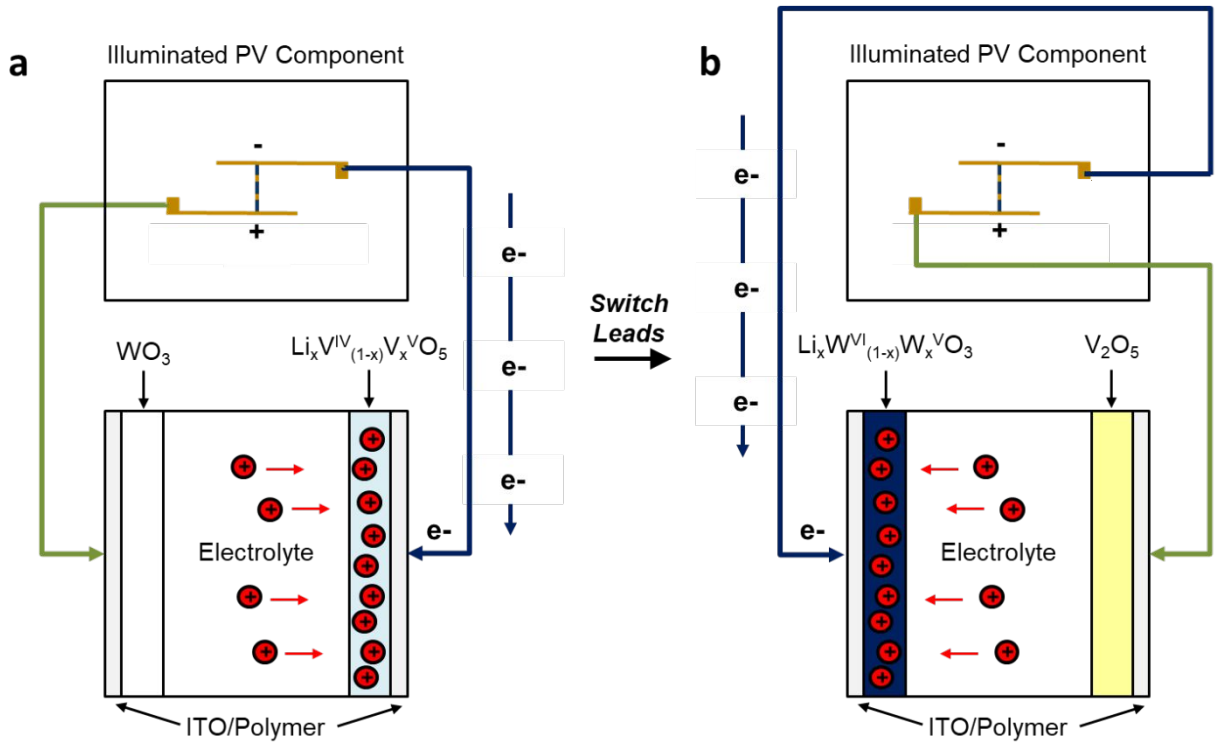

Figure 5. Schematic showing mechanism for color change within the PEC module. The illuminated PV component drives (a) bleaching and (b) coloration via the photovoltage generated by the Si μ-cell array.

flexible, polyethylene terephthalate (PET) substrate with an area of 5 cm x 4 cm. The EC device is prepared as described above, with an area of 1.2 cm x 1.2 cm. To drive the EC component to the bleached state, the illuminated PV component is connected to the EC component according to **Figure 5a**. The applied photovoltage results in diffusion of Li^+ to the V_2O_5-based electrode, resulting in reduction and oxidation of the V_2O_5 and WO_3 films, respectively. Similarly, as shown in **Figure 5b**, the absorptive state is realized by switching the leads on the EC component electrodes; upon switching the leads, the direction of the bias supplied by the illuminated PV component photovoltage is reversed, and Li^+ diffuse to the WO_3-based electrode, resulting in reduction and oxidation of the WO_3 and V_2O_5 films, respectively.

The μ-cells are planarized in NOA61 prior to interconnection, and this gives rise to an increase in J_{SC} due to short-range waveguiding effects.[28] Effects of illuminated waveguide area on J_{SC} are shown in **Figure S12a**, which is correlated with a decreased EC device switching time at constant EC device area (**Figure S12b**). This implies that a larger waveguide area, and thus a lower density of Si μ-cells, is preferable for powering the EC device. In practice, the waveguide will scale with EC area, and the benefit is outweighed by the additional charge needed for the larger EC area (**Figure S12c**). Waveguides that typically benefit from enlarged areas, such as luminescent solar concentrators, are also burdened by the additional charge with increased EC area. While concentration effects do decrease overall switching time, **Figure S12d** shows a similar trend to that of **Figure S12c**.

Figure 6a depicts the PEC prototype, and **Figure 6b** shows the change in transmission for PEC device powered by two Si μ-cells in series. Powered by these two cells, the transmission is modulated with a consistent ΔT_{max} of about 30-40%. As seen in **Figure 6c**, coloration and bleaching times can also be calculated for the PEC device by cycling between bleached and absorptive states. Here, the bias was held for 6 minutes and transmission at 600 nm was monitored before switching the leads. A coloration time of 160.9 seconds and a bleaching time of 179.4 seconds are observed for our PEC device, with a ΔT_{max} of 32%. The device also displays memory, as seen in **Figure S13(a-b)** in the Supplementary Information. The Si μ-cell leads were attached to the EC device for 6 minutes and then disconnected to continually measure transmission thereafter. There is a slight increase/decrease in transmission of ca. 2% for the absorptive/bleached states after the bias from the Si μ-cells is removed.

Figure 6c summarizes the coloration and bleaching times for 1, 0.79, 0.50, and 0.25 suns, corresponding to times of day when there is less than 1 sun irradiation on the window of a

building. As expected, with decreased irradiation (i.e., decreased current) the switching times increase. The theoretical values plotted (shown in black) are calculated based on the amount of injected charge and expected J_{SC} values, assuming the μ-cell J_{SC} is constantly provided to the EC device. The experimental coloration times agree well with the modelling predictions; the bleaching times show some deviations at low intensity likely due to asymmetric charge injection and extraction processes, as discussed above. Regardless of intensity, the magnitude of the limiting transmission modulation is dictated by the magnitude of the applied bias, or μ-cell V_{OC}. **Figure S13c** in the Supplementary Information confirms this notion and shows transmission spectra of the PEC device at each intensity, wherein each spectrum displays similar modulation in transmission over the wavelength range. **Figure S13(d-e)** shows the expected transmission values for bleaching and coloration at 3 minutes after the bias was applied, further illustrating the effect of illumination intensity on switching times.

There are multiple ways to decrease the switching times of the PEC device, the most impactful of which is adding additional Si μ-cells in parallel to increase the J_{SC} (i.e., increasing μ-cell density), although the additional μ-cells could reduce the transparency of the device. For large pitch configurations, however, these impacts can be quite small as illustrated by the data in **Figure 6d** which shows the transmission of two and four Si μ-cells corresponding to one and two pairs of Si μ-cells in parallel in the current design (i.e., a pair of two Si μ-cells in series). The additional μ-cells only reduce transmission by ca. 2% while doubling the J_{SC}, reducing the switching time from 152 to 76 seconds. Thus, the benefit of increased μ-cell density on EC device switching time could outweigh the resulting decrease in transmission of the overall PEC device. Similarly, without significant adverse impact to the average visible transmittance (AVT)[3] of the PEC device as a whole, increasing the quantity of μ-cells in series per unit area of EC

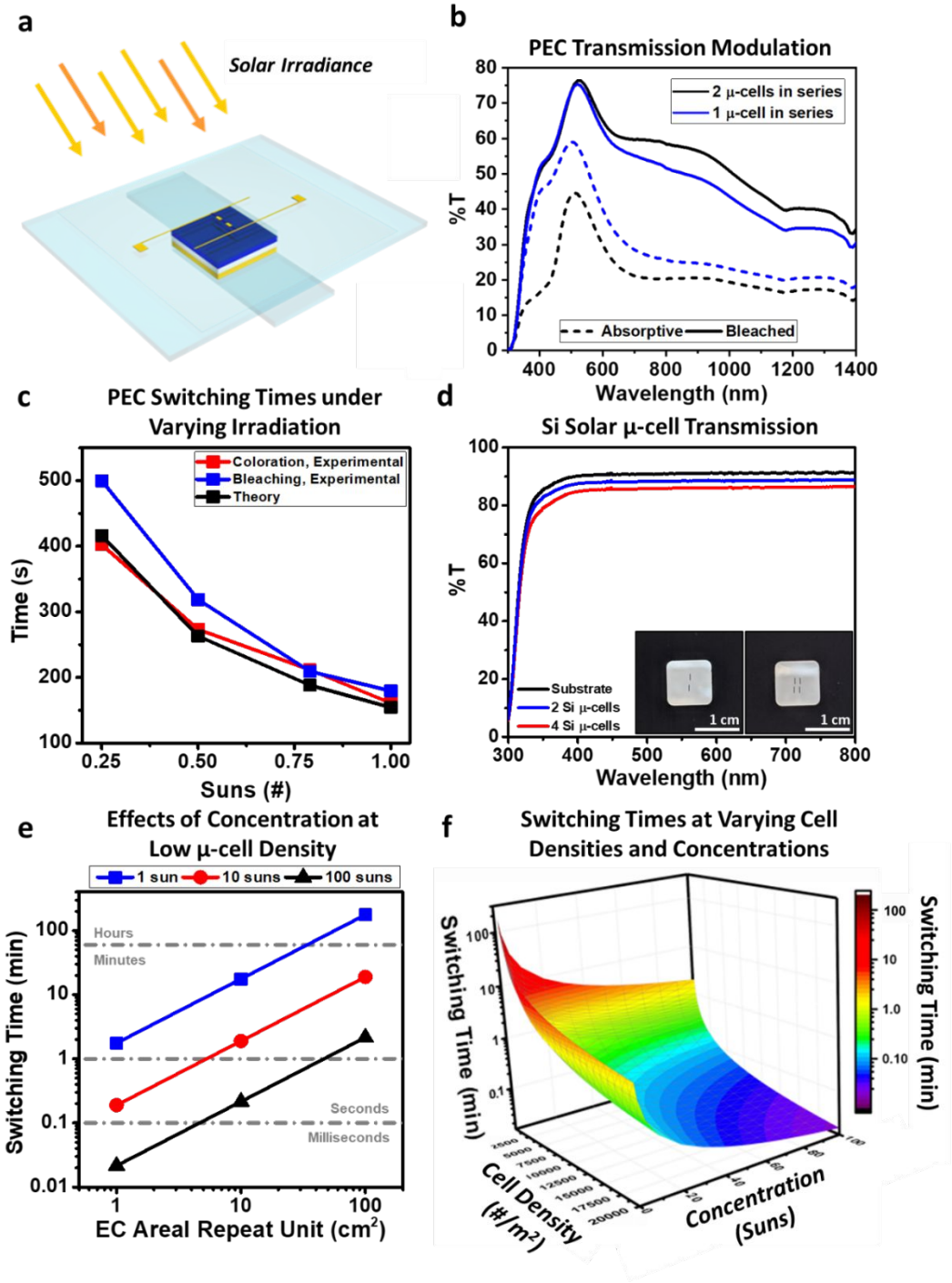

Figure 6. (a) Schematic of the PEC device. (b) Transmission of the PEC device powered by one (blue) and two (black) Si μ-cells in series in the bleached (solid line) and absorptive (dashed line) states. (c) Calculated switching times for coloration (red), bleaching (blue) and theoretical values (black) for varying irradiation. (d) Transmission for two (blue) and four (red) Si μ-cells compared to the substrate (black). Images of the Si μ-cells are shown in the inset. (e-f) Calculated switching times for varying Si μ-cell density and concentration (e) for our 1 cm^2 device and (f) for larger devices on the order of m^2.

device would allow for higher transmission modulation of the EC component (larger applied bias via μ-cell V_{OC}). This approach in tandem with the application of thicker electrochromic and ion storage layer films would result in improved coloration efficiency at larger applied biases.

In addition to increasing μ-cell density, switching times can also be reduced through light concentration, as demonstrated in **Figure 6e**. Here, a larger EC areal repeat unit corresponds to a larger active EC area powered by two Si μ-cells in series (i.e., reduced μ-cell density). Reduced μ-cell density is beneficial from a cost perspective; as the magnitude of the EC areal repeat unit is increased (i.e., μ-cell density is decreased), the switching time of the EC device increases for a given concentration, but less active PV material is consumed. At high EC areal repeat unit sizes (low μ-cell densities), however, the decrease in switching time can be recovered by increasing the light concentration. For example, as shown in **Figure 6e**, an EC repeat unit of 100 cm^2 under 1 sun (shown in blue) has a switching time on the order of hours, but a fast switching time (i.e., on the order of minutes) can be recovered through concentration at 100 suns (shown in black). Concentration also increases the V_{OC} logarithmically and can therefore also increase the maximum modulation in transmission. This was accounted for in the switching time calculations and details can be found in **Figure S14** in the Supplementary Information. Combining these two strategies (i.e., μ-cell density and light concentration) to manipulate switching times, **Figure 6f** provides a guide to fabricating a PEC device for windows on the meter scale with a desired switching time. One axis corresponds to increased cell density, or increased μ-cells in parallel (# m^{-2}, or number of μ-cells per unit area of EC device). The other axis employs concentration to decrease switching times. Any combination of these two can be used to balance overall transmission, cost, and switching times of PEC windows. As seen in the figure, it is realistic to achieve switching times less than 1 minute for a reasonable amount of Si μ-cells and modest

degrees of light concentration. To optimize μ-cell density for large scale application comprehensively, the influence of μ-cell density on switching time, overall transparency, and module production cost would need to be considered.

2.3.3. Flexible Electrochromic Device Performance

In complement to the device architecture shown in **Figure 2a** and **Figure 6a**, the flexibility of the PV component prepared on a PET substrate is pictorially demonstrated in **Figure S15a**, and an example image of a PEC device prototype on flexible substrates is shown in **Figure S15b**. To evaluate performance in modules subject to flexure, we fabricated a full device pixel module (rendered image in **Figure 2a**) on ITO-coated Corning® Willow® glass (100 μm thick) and cycled the device between flat and bent states using a Dynamic Mechanical Analysis (DMA) instrument with a 3-point flexural test setup, as shown in **Figure 7(a-b)**. After cycling the EC device 50 times with forces upwards of 1200 g (a load just below the fracture point of the glass yielding a vertical displacement of 0.3 mm, **Figure S16**), we saw strains of this magnitude were subject to creep that resulted in small amounts of permanent deformation. This is evident in the data shown in **Figure S16**. Irrespective of this irreversible degree of strain, we observed very little change in the transmission spectrum seen in the absorptive and bleached states (**Figure 7c**, with an applied bias of 1.0 V). After bending, the ΔT_{max} and η of the EC device decreased by 1.3 % and 6.2 %, respectively (**Table S2**), which further illustrates the small influence of bending and applied stress on EC device performance. We also monitored switching times for coloration and bleaching as determined from cycling the EC device with a 1.0 V bias while monitoring transmission at 600 nm (**Figure 7d**). These times were comparable before and after bending and were also comparable to device performance on non-flexible substrates as previously measured (**Table S2 cf. Table 1**). Taken together, these results suggest promise for materials better optimized for compatibility with large-scale roll-to-roll processing (most notably

for the electrolyte phase) to afford high electro-optical performances in PECs with robust degrees of flexural stability.

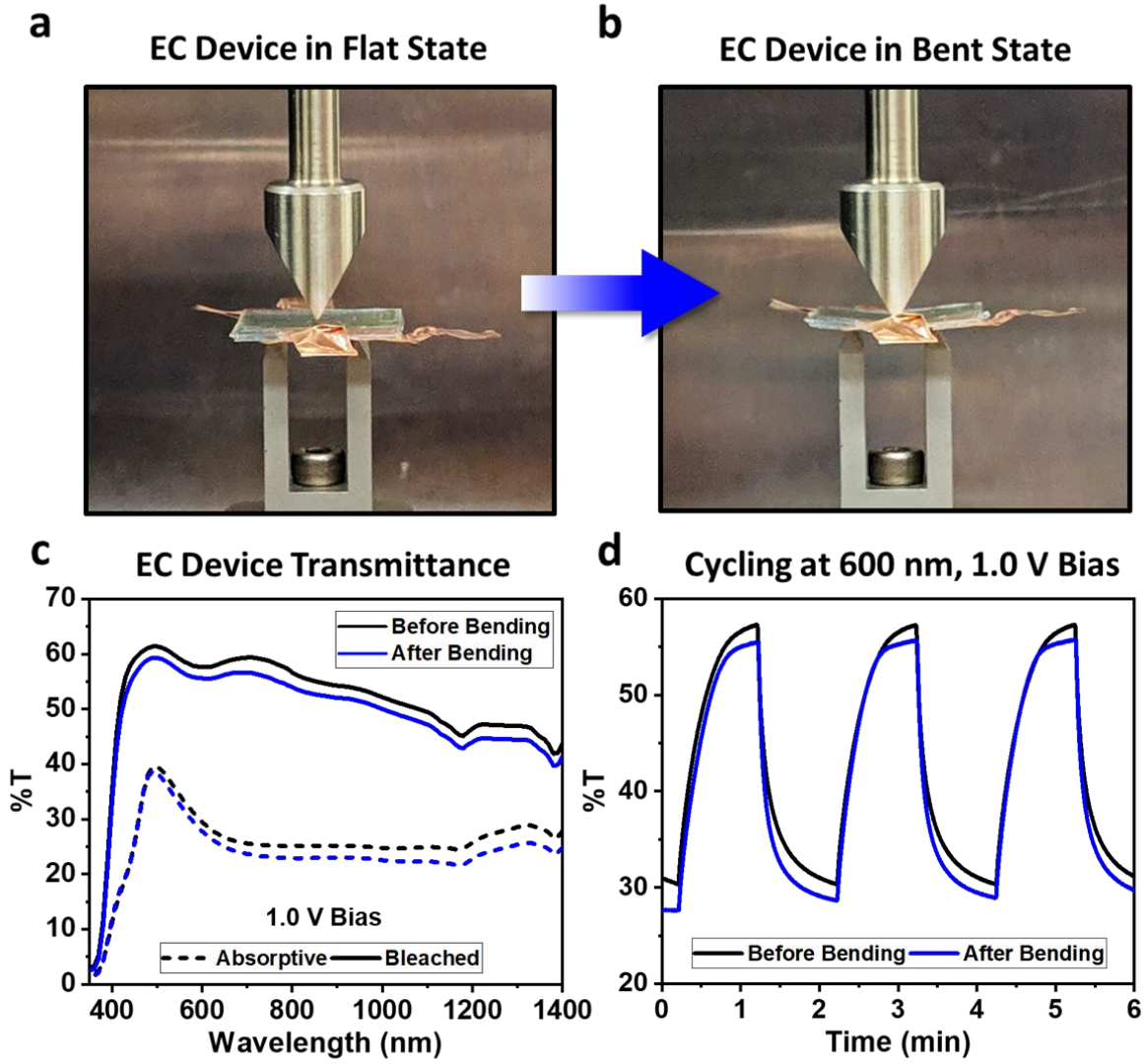

Figure 7. Images of the 3-point flexural test setup for the flexible EC device in (a) a flat and (b) bent state. (c) Transmission spectra of the EC device before (black) and after (blue) bending. (d) EC device cycling between +/- 1.0 V monitored at 600 nm before (black) and after (blue) bending.

2.4. Conclusion

The current work describes a prototype of a device that takes advantage of the unique attributes of high photovoltaic performance Si μ-cells.[18] The ability to integrate relatively transparent, single-crystalline materials with EC thin film devices provides an intriguing approach to

construct autonomous (i.e., self-powered) smart windows with high performance and long lifetimes. The materials attributes of the designs shown afford notable points of distinction and contrast with self-powered window designs based on polymeric or organic PV materials. Additionally, in contrast to side-by-side PEC or edge-lined technologies, the micro-PV array form factor allows for enhanced J_{SC} by short-range waveguiding effects to the PV device edges afforded by planarization in NOA, and the implementation of ultrathin Si PV minimizes large-scale production costs by virtue of their fabrication via "kerf-free" methods[54-58] relative to conventional wafering techniques.[35, 59] We further show materials processed via sol-gel methods that are easily fabricated and scaled as functional thin films, a gel electrolyte that displays high ionic conductivity with desirable mechanical properties, and potential for fabrication on flexible substrates that are compatible with roll-to-roll processing. The combination of these electrochromic materials shows impressive performance with a ΔT_{max} as high as 33% and fast switching times as low as 8 seconds for modulation at 600 nm. With high transmission and the ability to place the μ-cells nearly anywhere in the window area, switching times of less than 3 minutes are achieved with ΔT_{max} of 32% for two Si μ-cells connected in series (1.12 V). Switching times can be addressed either via Si μ-cell density corresponding to additional μ-cells in parallel, or via concentration. Future work aims to optimize electrochromic layer materials selection and thickness for performance with the Si μ-cell array. These strategies illustrate pathways toward full PEC-based prototypes of functional smart windows on the building-scale with similar modulation in transmission and fast switching times.

Supporting Information

Experimental methods, materials characterization, Si solar microcell fabrication and testing, additional electrochromic device characterization, and additional photoelectrochromic device

characterization is available in the supporting information. Also available is a video of the assembled electrochromic device cycling from the bleached to the absorptive state. University logo in video used with permission from the University of Illinois.

Corresponding Author

*Ralph G. Nuzzo

r-nuzzo@illinois.edu

Author Contributions

The manuscript was written through contributions of all authors. All authors have given approval to the final version of the manuscript. †Authors contributed equally to the work.

Acknowledgements

The development of the materials chemistries and device form factors for autonomous electrochromic systems integrating high-performance microcell materials was carried out with support from the "Photonics at Thermodynamic Limits" Energy Frontier Research Center funded by the U.S. Department of Energy, Office of Science, Office of Basic Energy Sciences under Award Number DE-SC0019140. This work exploits microcell PV materials developed with the support of the "Light-Material Interactions in Energy Conversion" Energy Frontier Research Center funded by the U.S. Department of Energy, Office of Science, Office of Basic Energy Sciences under Award Number DE-SC0001293 (subcontract no. 67N-1087758). The experiments used the facilities at the Materials Research Laboratory and Center for Microanalysis of Materials at the University of Illinois at Urbana-Champaign. Dynamic Mechanical Analysis (DMA) was performed by Leon Dean in the Sottos Research Group at the University of Illinois at Urbana Champaign, Department of Materials Science and Engineering. Maggie M. Potter and Mikayla A. Yoder contributed equally to this work.

References

1. Davy, N. C.; Sezen-Edmonds, M.; Gao, J.; Lin, X.; Liu, A.; Yao, N.; Kahn, A.; Loo, Y.-L. Pairing of Near-Ultraviolet Solar Cells with Electrochromic Windows for Smart Management of the Solar Spectrum. *Nat. Energy* **2017,** *2* (8), 1-10.
2. Korgel, B. A. Composite for Smarter Windows. *Nature* **2013,** *500*, 278.
3. Traverse, C. J.; Pandey, R.; Barr, M. C.; Lunt, R. R. Emergence of Highly Transparent Photovoltaics for Distributed Applications. *Nat. Energy* **2017,** *2* (11), 849-860.
4. U.S. Energy Information Administration, 2012.
5. Wang, Y.; Runnerstrom, E. L.; Milliron, D. J. Switchable Materials for Smart Windows. *Annu. Rev. Chem. and Biomol. Eng.* **2016,** *7* (1), 283-304.
6. Shehabi, A.; DeForest, N.; McNeil, A.; Masanet, E.; Greenblatt, J.; Lee, E. S.; Masson, G.; Helms, B. A.; Milliron, D. J. U.S. Energy Savings Potential from Dynamic Daylighting Control Glazings. *Energy and Buildings* **2013,** *66*, 415-423.
7. DeForest, N.; Shehabi, A.; O'Donnell, J.; Garcia, G.; Greenblatt, J.; Lee, E. S.; Selkowitz, S.; Milliron, D. J. United States Energy and CO_2 Savings Potential from Deployment of Near-Infrared Electrochromic Window Glazings. *Building and Environment* **2015,** *89*, 107-117.
8. Deb, S. K. A Novel Electrophotographic System. *Appl. Opt.* **1969,** *8* (S1), 192-195.
9. Deb, S. K. *The Philosophical Magazine: A Journal of Theoretical Experimental and Applied Physics* **1973,** *27,* 801-822.
10. Platt, J. R. Electrochromism, a Possible Change of Color Producible in Dyes by an Electric Field. *J. Chem. Phys.* **1961,** *34* (3), 862-863.
11. Faughnan, B. W.; Crandall, R. S. *Display Devices*; Springer: Berlin, 1980; Vol. 40., pp 181-211.
12. Schuster, A. P.; Nguyen, D.; Caporaletti, O. Solid State Electrochromic Infrared Switchable Windows. *Sol. Energy Mater.* **1986,** *13* (2), 153-160.
13. Bechinger, C.; Bullock, J. N.; Zhang, J. G.; Tracy, C. E.; Benson, D. K.; Deb, S. K.; Branz, H. M. Low-Voltage Electrochromic Device for Photovoltaic-Powered Smart Windows. *J. Appl. Phys.* **1996,** *80* (2), 1226-1232.
14. Benson, D. K.; Branz, H. M. Design Goals and Challenges for a Photovoltaic-Powered Electrochromic Window Covering. *Sol. Energy Mater. Sol. Cells* **1995,** *39* (2), 203-211.
15. Cui, M.-H.; Guo, J.-S.; Xie, H.-Q.; Wu, Z.-H.; Qiu, S.-C. All-Solid-State Complementary Electrochromic Windows Based on the Oxymethylene-Linked Polyoxyethylene Complexed with $Liclo_4$. *J. Appl. Polym. Sci.* **1997,** *65* (9), 1739-1744.
16. Deb, S. K.; Lee, S.-H.; Edwin Tracy, C.; Roland Pitts, J.; Gregg, B. A.; Branz, H. M. Stand-Alone Photovoltaic-Powered Electrochromic Smart Window. *Electrochim. Acta* **2001,** *46* (13), 2125-2130.
17. Piccolo, A.; Simone, F. Performance Requirements for Electrochromic Smart Window. *Journal of Building Engineering* **2015,** *3*, 94-103.
18. Yoder, M. A.; Yao, Y.; He, J.; Nuzzo, R. G. Optimization of Photon and Electron Collection Efficiencies in Silicon Solar Microcells for Use in Concentration-Based Photovoltaic Systems. *Adv. Mater. Technol.* **2017,** *2* (11), 1-9.
19. Huang, L.-M.; Hu, C.-W.; Liu, H.-C.; Hsu, C.-Y.; Chen, C.-H.; Ho, K.-C. Photovoltaic Electrochromic Device for Solar Cell Module and Self-Powered Smart Glass Applications. *Sol. Energy Mater. Sol. Cells* **2012,** *99*, 154-159.

20. Huang, L.-M.; Hu, C.-W.; Peng, C.-Y.; Su, C.-H.; Ho, K.-C. Integration of Polyelectrolyte Based Electrochromic Material in Printable Photovoltaic Electrochromic Module. *Sol. Energy Mater. Sol. Cells* **2016,** *145*, 69-75.
21. Ghosh, A.; Norton, B.; Duffy, A. First Outdoor Characterisation of a PV Powered Suspended Particle Device Switchable Glazing. *Sol. Energy Mater. Sol. Cells* **2016,** *157*, 1-9.
22. Dyer, A. L.; Bulloch, R. H.; Zhou, Y.; Kippelen, B.; Reynolds, J. R.; Zhang, F. A Vertically Integrated Solar-Powered Electrochromic Window for Energy Efficient Buildings. *Adv. Mater.* **2014,** *26* (28), 4895-900.
23. Milliron, D. J. Ultraviolet Photovoltaics: Share the Spectrum. *Nat. Energy* **2017,** *2* (8), 17116.
24. Kwon, H.-K.; Lee, K.-T.; Hur, K.; Moon, S. H.; Quasim, M. M.; Wilkinson, T. D.; Han, J.-Y.; Ko, H.; Han, I.-K.; Park, B.; Min, B. K.; Ju, B.-K.; Morris, S. M.; Friend, R. H.; Ko, D.-H. Optically Switchable Smart Windows with Integrated Photovoltaic Devices. *Adv. Energy Mater.* **2015,** *5* (3), 1401347.
25. Martina, F.; Pugliese, M.; Serantoni, M.; Baldisserri, C.; Gorni, G.; Maggiore, A.; Gigli, G.; Maiorano, V. Large Area Self-Powered Semitransparent Trifunctional Device Combining Photovoltaic Energy Production, Lighting and Dynamic Shading Control. *Sol. Energy Mater. Sol. Cells* **2017,** *160*, 435-443.
26. Wu, C.-C.; Liou, J.-C.; Diao, C.-C. Self-Powered Smart Window Controlled by a High Open-Circuit Voltage InGaN/GaN Multiple Quantum Well Solar Cell. *Chem. Commun.* **2015,** *51* (63), 12625-12628.
27. Cannavale, A.; Eperon, G. E.; Cossari, P.; Abate, A.; Snaith, H. J.; Gigli, G. Perovskite Photovoltachromic Cells for Building Integration. *Energy Environ. Sci.* **2015,** *8* (5), 1578-1584.
28. Meitl, M. A.; Zhu, Z.-T.; Kumar, V.; Lee, K. J.; Feng, X.; Huang, Y. Y.; Adesida, I.; Nuzzo, R. G.; Rogers, J. A. Transfer Printing by Kinetic Control of Adhesion to an Elastomeric Stamp. *Nat. Mater.* **2005,** *5* (1), 33-38.
29. Feng, X.; Meitl, M. A.; Bowen, A. M.; Huang, Y.; Nuzzo, R. G.; Rogers, J. A. Competing Fracture in Kinetically Controlled Transfer Printing. *Langmuir* **2007,** *23* (25), 12555-12560.
30. Kim, T.-H.; Carlson, A.; Ahn, J.-H.; Won, S. M.; Wang, S.; Huang, Y.; Rogers, J. A. Kinetically Controlled, Adhesiveless Transfer Printing Using Microstructured Stamps. *Appl. Phys. Lett.* **2009,** *94* (11), 113502.
31. Park, S.-I.; Xiong, Y.; Kim, R.-H.; Elvikis, P.; Meitl, M.; Kim, D.-H.; Wu, J.; Yoon, J.; Yu, C.-J.; Liu, Z.; Huang, Y.; Hwang, K.-c.; Ferreira, P.; Li, X.; Choquette, K.; Rogers, J. A. Printed Assemblies of Inorganic Light-Emitting Diodes for Deformable and Semitransparent Displays. *Science* **2009,** *325* (5943), 977-981.
32. Kim, H.-s.; Brueckner, E.; Song, J.; Li, Y.; Kim, S.; Lu, C.; Sulkin, J.; Choquette, K.; Huang, Y.; Nuzzo, R. G.; Rogers, J. A. Unusual Strategies for Using Indium Gallium Nitride Grown on Silicon (111) for Solid-State Lighting. *Proc. Natl. Acad. Sci. U. S. A.* **2011,** *108* (25), 10072-10077.
33. Carlson, A.; Bowen, A. M.; Huang, Y.; Nuzzo, R. G.; Rogers, J. A. Transfer Printing Techniques for Materials Assembly and Micro/Nanodevice Fabrication. *Adv. Mater.* **2012,** *24* (39), 5284-5318.
34. Bronstein, N. D.; Li, L.; Xu, L.; Yao, Y.; Ferry, V. E.; Alivisatos, A. P.; Nuzzo, R. G. Luminescent Solar Concentration with Semiconductor Nanorods and Transfer-Printed Micro-Silicon Solar Cells. *ACS Nano* **2014,** *8* (1), 44-53.

35. Yao, Y.; Brueckner, E.; Li, L.; Nuzzo, R. Fabrication and Assembly of Ultrathin High-Efficiency Silicon Solar Microcells Integrating Electrical Passivation and Anti-Reflection Coatings. *Energy Envir. Sci.* **2013,** *6* (10), 3071-3079.
36. Bohnke, O.; Frand, G.; Rezrazi, M.; Rousselot, C.; Truche, C. Fast Ion Transport in New Lithium Electrolytes Gelled with PMMA. 1. Influence of Polymer Concentration. *Solid State Ionics* **1993,** *66* (1), 97-104.
37. Livage, J.; Ganguli, D. Sol–Gel Electrochromic Coatings and Devices: A Review. *Sol. Energy Mater. Sol. Cells* **2001,** *68* (3), 365-381.
38. Xie, F. Y.; Gong, L.; Liu, X.; Tao, Y. T.; Zhang, W. H.; Chen, S. H.; Meng, H.; Chen, J. XPS Studies on Surface Reduction of Tungsten Oxide Nanowire Film By Ar^+ Bombardment. *J. Electron. Spectrosc. Relat. Phenom.* **2012,** *185* (3), 112-118.
39. Biesinger, M. C.; Lau, L. W. M.; Gerson, A. R.; Smart, R. S. C. Resolving Surface Chemical States in XPS Analysis of First Row Transition Metals, Oxides and Hydroxides: Sc, Ti, V, Cu and Zn. *Appl. Surf. Sci.* **2010,** *257* (3), 887-898.
40. Zilberberg, K.; Trost, S.; Meyer, J.; Kahn, A.; Behrendt, A.; Lützenkirchen-Hecht, D.; Frahm, R.; Riedl, T. Inverted Organic Solar Cells with Sol–Gel Processed High Work-Function Vanadium Oxide Hole-Extraction Layers. *Adv. Funct. Mater.* **2011,** *21* (24), 4776-4783.
41. Sakunthala, A.; Reddy, M. V.; Selvasekarapandian, S.; Chowdari, B. V. R.; Selvin, P. C. Energy Storage Studies of Bare and Doped Vanadium Pentoxide, $(V_{1.95}M_{0.05})O_5$, M = Nb, Ta, for Lithium Ion Batteries. *Energy Environ. Sci.* **2011,** *4* (5), 1712-1725.
42. Hassab, S.; Shen, D. E.; Österholm, A. M.; Reynolds, J. R.; Padilla, J. Exploring Unbalanced Electrode Configurations for Electrochromic Devices. *J. Mater. Chem. C* **2018,** *6* (2), 393-400.
43. Zhang, J.; Tu, J. P.; Xia, X. H.; Qiao, Y.; Lu, Y. An All-Solid-State Electrochromic Device Based on Nio/WO_3 Complementary Structure and Solid Hybrid Polyelectrolyte. *Sol. Energy Mater. Sol. Cells* **2009,** *93* (10), 1840-1845.
44. Kuo, T.-H.; Hsu, C.-Y.; Lee, K.-M.; Ho, K.-C. All-Solid-State Electrochromic Device Based on Poly(Butyl Viologen), Prussian Blue, and Succinonitrile. *Sol. Energy Mater. Sol. Cells* **2009,** *93* (10), 1755-1760.
45. Wang, H.; Yan, M.; Jiang, Z. Electrochromic Properties of Rhodium Oxide Films Prepared by a Sol–Gel Method. *Thin Solid Films* **2001,** *401* (1), 211-215.
46. Xue, J.; Zhu, Y.; Jiang, M.; Su, J.; Liu, Y. Electrochromic WO_3 Thin Films Prepared by Combining Ion-Beam Sputtering Deposition with Post-Annealing. *Mater. Lett.* **2015,** *149*, 127-129.
47. Na, S.-I.; Kim, S.-S.; Jo, J.; Kim, D.-Y. Efficient and Flexible ITO-Free Organic Solar Cells Using Highly Conductive Polymer Anodes. *Adv. Mater.* **2008,** *20* (21), 4061-4067.
48. Skotheim, T. A.; Reynolds, J.; Elsenbamer, R. *Handbook of Conducting Polymers;* Marcel Dekker: New York; 1998.
49. Vosgueritchian, M.; Lipomi, D. J.; Bao, Z. Highly Conductive and Transparent PEDOT:PSS Films with a Fluorosurfactant for Stretchable and Flexible Transparent Electrodes. *Adv. Funct. Mater.* **2012,** *22* (2), 421-428.
50. Bae, S.; Kim, H.; Lee, Y.; Xu, X.; Park, J.-S.; Zheng, Y.; Balakrishnan, J.; Lei, T.; Ri Kim, H.; Song, Y. I.; Kim, Y.-J.; Kim, K. S.; Özyilmaz, B.; Ahn, J.-H.; Hong, B. H.; Iijima, S. Roll-to-Roll Production of 30-Inch Graphene Films for Transparent Electrodes. *Nat. Nanotechnol.* **2010,** *5*, 574.

51. Zhang, D.; Ryu, K.; Liu, X.; Polikarpov, E.; Ly, J.; Tompson, M. E.; Zhou, C. Transparent, Conductive, and Flexible Carbon Nanotube Films and Their Application in Organic Light-Emitting Diodes. *Nano Lett.* **2006,** *6* (9), 1880-1886.
52. Hu, L.; Kim, H. S.; Lee, J.-Y.; Peumans, P.; Cui, Y. Scalable Coating and Properties of Transparent, Flexible, Silver Nanowire Electrodes. *ACS Nano* **2010,** *4* (5), 2955-2963.
53. Judeinstein, P.; Morineau, R.; Livage, J. Electrochemical Degradation of $WO_3 \cdot nH_2O$ Thin Films. *Solid State Ionics* **1992,** *51* (3), 239-247.
54. Dross, F.; Robbelein, J.; Vandevelde, B.; Van Kerschaver, E.; Gordon, I.; Beaucarne, G.; Poortmans, J. Stress-Induced Large-Area Lift-Off of Crystalline Si Films. *Appl. Phys. A* **2007,** *89* (1), 149-152.
55. Depauw, V.; Gordon, I.; Beaucarne, G.; Poortmans, J.; Mertens, R.; Celis, J.-P. Large-Area Monocrystalline Silicon Thin Films by Annealing of Macroporous Arrays: Understanding and Tackling Defects in yhe Material. *J. Appl. Phys.* **2009,** *106* (3), 033516.
56. Green, M. A.; Basore, P. A.; Chang, N.; Clugston, D.; Egan, R.; Evans, R.; Hogg, D.; Jarnason, S.; Keevers, M.; Lasswell, P.; O'Sullivan, J.; Schubert, U.; Turner, A.; Wenham, S. R.; Young, T. Crystalline Silicon on Glass (CSG) Thin-Film Solar Cell Modules. *Sol. Energy* **2004,** *77* (6), 857-863.
57. Song, D.; Inns, D.; Straub, A.; Terry, M. L.; Campbell, P.; Aberle, A. G. Solid Phase Crystallized Polycrystalline Thin-Films on Glass from Evaporated Silicon for Photovoltaic Applications. *Thin Solid Films* **2006,** *513* (1), 356-363.
58. Terry, M. L.; Straub, A.; Inns, D.; Song, D.; Aberle, A. G. Large Open-Circuit Voltage Improvement by Rapid Thermal Annealing of Evaporated Solid-Phase-Crystallized Thin-Film Silicon Solar Cells on Glass. *Appl. Phys. Lett.* **2005,** *86* (17), 172108.
59. Rodriguez, H.; Guerrero, I.; Koch, W.; Endrös, A. L.; Franke, D.; Häßler, C.; Kalejs, J. P.; Möller, H. J. *Handbook of Photovoltaic Science and Engineering*; John Wiley & Sons: 2011; pp 218-264.

Table of Contents Image